Pergamon

Int. J. Heat Mass Transfer. Vol. 37, No. 13, pp. 1857–1866, 1994

0017–9310/94 $7.00 + 0.00

0017–9310(94)E0020–U

Mixed convection heat and mass transfer in inclined rectangular ducts

WEI-MON YAN

Department of Mechanical Engineering, Hua Fan College of Humanities and Technology, Shih Ting, Taipei, Taiwan 22305, Republic of China

(*Received* 17 *August* 1993 *and in final form* 29 *December* 1993)

Abstract—A numerical study was made to investigate the laminar mixed convection heat and mass transfer in inclined rectangular ducts. Using the vorticity–velocity method, three-dimensional Navier–Stokes equations, the energy and concentration equations were solved simultaneously. Six independent parameters are introduced: Prandtl number Pr, mixed convection parameter Ω, modified Rayleigh number Ra^*, buoyancy ratio N, aspect ratio γ and Schmidt number Sc. The numerical results, including the local friction factor ratio, local Nusselt and Sherwood numbers, are presented for species diffusion of interest in air ($Pr = 0.7$) over a Schmidt number range of $Sc = 0.2$–2.0. In the study, the mixed convection parameter Ω ranges from 0 to 200, while the modified Rayleigh numbers Ra^* are varied from 0 to 10^5 for the aspect ratios $\gamma = 0.5$, 1, and 2.0 with buoyancy ratios N ranging from -0.5 to 2.0. The results show that the buoyancy effects have a significant influence on the characteristics of fluid flow, heat and mass transfer. Additionally, the $fRe/(fRe)_0$, Nu and Sh are enhanced as the buoyancy force from species diffusion assists the thermal buoyancy force.

INTRODUCTION

SITUATIONS often arise in which the combined buoyancy forces of thermal and mass transfer, resulting from the simultaneous presence of differences in temperature and concentration, have rather significant influences on the velocity, temperature and concentration profiles and the associated friction, heat and mass transfer coefficients in ducts. Outstanding examples include the chemical distillatory processes, design of heat exchangers, channel type solar energy collectors and thermo-protection systems. For vertical ducts, the gravity force acts in the main flow direction, and there is no secondary flow in the cross-section. For horizontal ducts, the combined buoyancy forces are normal to the main flow direction and they induce secondary flows in the cross-section. In inclined ducts, however, buoyancy forces act in both the main flow and the cross-stream directions.

The fully-developed mixed convection heat transfer has been investigated for the flow in horizontal ducts [1, 2] and in inclined ducts [3–6]. Mixed convection in the thermal entrance region of horizontal rectangular channels under the assumption of large Prandtl number were studied by Cheng *et al.* [7] and Ou *et al.* [8]. The same problems were also investigated for a horizontal tube by Hieber and Sreenivasan [9], Ou and Cheng [10] and Hishida *et al.* [11]. But these results are applicable only to the fluids of large Prandtl number. Without the assumption of a large Prandtl number, the detailed numerical studies on mixed convection heat transfer have been studied in horizontal ducts [12–18]. In many practical situations, the duct is not horizontal and the problems of mixed convection in inclined ducts become important. Abou-Ellail and Morcos [19] presented a numerical study of mixed convection heat transfer in an inclined channel. Photographs of developing secondary flow patterns in the thermal entrance region of inclined tubes for laminar mixed convection flow were presented by Cheng and Yuen [20]. An experimental study on mixed convection heat transfer in the entrance region of inclined rectangular ducts was carried out by Morcos *et al.* [21]. In ref. [21], an aluminum rectangular channel was used as a test section. Therefore, the wall conduction effect plays an important role in their studies. Choudhury and Patankar [22] performed an analysis of the combined forced and free convection for laminar flow in the entrance region of isothermal, inclined tubes. Their results revealed that buoyancy effects have a considerable influence on the fluid flow and heat transfer characteristics of the development flow.

As far as mixed convection heat and mass transfer are concerned, Santarelli and Foraboschi [23] investigated the buoyancy effects of thermal and mass diffusion on laminar forced convection flow undergoing a chemical reaction. Mixed convection heat and mass transfer in vertical two-dimensional ducts was performed by Yan [24, 25]. In refs. [24, 25], Yan found that the combined buoyancy forces of thermal and solutal diffusion have considerable effects on laminar forced convection. Recently, mixed convection heat and mass transfer in a horizontal square duct has been studied by Lin *et al.* [26].

In spite of its importance in engineering applications, the mixed convection heat and mass transfer

NOMENCLATURE

A cross-sectional area of a horizontal rectangular duct [m^2]
a, b width and height of a rectangular duct [m]
c, C dimensional and dimensionless species concentration
D mass diffusivity
D_e equivalent hydraulic diameter, $4A/S$
f friction factor, $2\bar{\tau}_w/(\rho\bar{w}_f^2)$
g gravitational acceleration [m s^{-2}]
Gr Grashof number, $g\beta q''_w D_e^4/(v^2 k)$
$\bar{h}$ average heat transfer coefficient [W m^{-2} K^{-1}]
$\bar{h}_M$ average mass transfer coefficient
I, J number of finite difference divisions in X and Y directions
k thermal conductivity [W m K^{-1}]
m mth iteration
m''_w mass diffusion flux at the channel wall [kg m^2 s^{-1}]
N buoyancy ratio, $(\beta^* m''_w/D)/(\beta q''_w/k)$
n outward normal direction to the wall
Nu local Nusselt number, $\bar{h}D_e/k$
p_m dynamic pressure [kPa]
$\bar{p}$ cross-sectional mean pressure [kPa]
$\bar{P}$ dimensionless cross-sectional mean pressure
P' perturbation term about the mean pressure $\bar{P}$
Pr Prandtl number, v/α
q''_w uniform wall heat flux [W m^{-2}]
Ra Rayleigh number, $Pr\,Gr$
Ra^* modified Rayleigh number, $Ra\cos\delta$
Re Reynolds number, $\bar{w}_f D_e/v$
S circumference of cross section [m]
Sc Schmidt number, v/D
Sh Sherwood number, $\bar{h}_M D_e/D$
T temperature [K]
T_0 inlet temperature [K]
U, V, W dimensionless velocity components in X, Y and Z directions
w_f fully-developed axial velocity before the entrance [m s^{-1}]
W_f dimensionless fully-developed axial velocity before the entrance
$\bar{W}_f$ mean quantity for W_f
x, y, z rectangular coordinate [m]
X, Y, Z dimensionless rectangular coordinate, $X = x/D_e$, $Y = y/D_e$, $Z = z/(ReD_e)$
Z^* dimensionless z-direction coordinate, $z/(PrReD_e) = Z/Pr$.

Greek symbols

α thermal diffusivity [m^2 s^{-1}]
β coefficient of thermal expansion [K^{-1}]
β^* coefficient of concentration expansion
δ duct inclination angle
γ aspect ratio of a rectangular duct, a/b
θ dimensionless temperature, $(T-T_0)/q''_w D_e/k)$
v kinematic viscosity [m^2 s^{-1}]
ξ dimensionless vorticity in axial direction
ρ density [kg m^{-3}]
Ω mixed convection parameter, $(Ra/Re)\sin\delta$.

Subscripts

b bulk fluid quantity
f fully-developed quantity before thermal entrance
o condition for purely forced convection
w value at wall.

Superscript

$\bar{}$ average value.

in inclined rectangular ducts has not been well evaluated. This motivates the present investigation. The purpose of this study is to examine the effects of combined buoyancy forces of thermal and solutal diffusion on laminar forced convection in inclined rectangular ducts.

ANALYSIS

Problem statement

The inclined rectangular duct under consideration is shown schematically in Fig. 1 with an inclination angle δ. The u, v and w are the velocity components in the x, y and z directions, respectively. A fully-developed axial velocity profile w_f and a constant inlet temperature T_0 and concentration c_0 are imposed at the entrance $z = 0$. The duct walls are subjected to a uniform heat flux q''_w and uniform mass flux m''_w. The flow is assumed to be steady and have constant thermophysical properties except the buoyancy terms in the y and z momentum equations. It was shown in refs. [13, 15] that the axial diffusion terms in the governing equations are negligible when the Peclet number is greater than 100. The buoyancy force resulting from the concentration difference may assist or oppose the buoyancy force from the temperature variation in the fluid. Because of the symmetry inherent in the problem, the calculations can be restricted to a solution domain that comprises one-half of the inclined rectangular duct as shown in Fig. 1.

Governing equations

By using the equation of state for an ideal gas mixture and assuming a low level of concentration in the

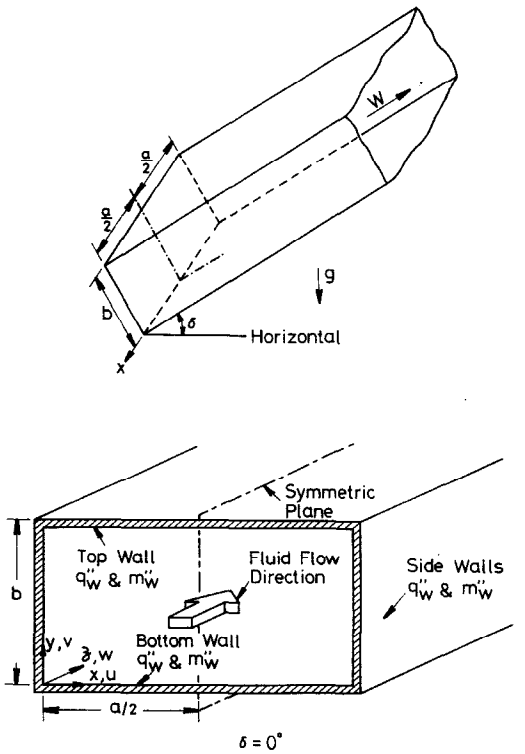

FIG. 1. Physical configuration and coordinate system.

flow, the density variation in the flow can be approximated by:

$$\rho = \rho_0 [1-\beta(T-T_0)-\beta^*(c-c_0)] \quad (1)$$

where ρ_0 is the density evaluated at the reference temperature T_0 and concentration c_0.

In order to determine the governing parameters, the momentum, energy, and concentration equations for laminar flow are normalized. The independent and dependent variables are non-dimensionalized by their characteristic quantities as follows:

$$X = x/D_e \qquad Y = y/D_e$$
$$Z = z/(Re\, D_e) \qquad Z^* = Z/Pr$$
$$U = uD_e/\nu \qquad V = vD_e/\nu$$
$$W = w/\bar{w}_f \qquad \bar{P} = \bar{p}/(\rho_0 \bar{w}_f^2)$$
$$P' = p'/(\rho_0 \nu^2/D_e^2) \qquad \theta = (T-T_0)/(q''_w D_e/k)$$
$$C = (c-c_0)/(m''_w D_e/D) \qquad Gr = \beta q''_w D_e^4/(\nu^2 k)$$
$$Ra = Pr\, Gr \qquad N = (\beta^* m''_w/D)/(\beta q''_w/k)$$
$$Ra^* = Ra\cos\delta \qquad \Omega = (Ra/Re)\sin\delta$$
$$Pr = \nu/\alpha \qquad Sc = \nu/D$$
$$\gamma = a/b \qquad D_e = 4A/S. \quad (2)$$

With these definitions and the assumptions made earlier, the dimensionless governing equations can then be written as follows:

Continuity equation:

$$\partial U/\partial X+\partial V/\partial Y+\partial W/\partial Z = 0; \quad (3)$$

X-direction momentum equation:

$$U\partial U/\partial X+V\partial U/\partial Y+W\partial U/\partial Z$$
$$= -\partial P'/\partial X+\partial^2 U/\partial X^2+\partial^2 U/\partial Y^2; \quad (4)$$

Y-direction momentum equation:

$$U\partial V/\partial X+V\partial V/\partial Y+W\partial V/\partial Z$$
$$= -\partial P'/\partial Y+\partial^2 V/\partial X^2+\partial^2 V/\partial Y^2$$
$$+(Ra^*/Pr)(\theta+NC); \quad (5)$$

Z-direction momentum equation:

$$U\partial W/\partial X+V\partial W/\partial Y+W\partial W/\partial Z$$
$$= -\mathrm{d}\bar{P}/\mathrm{d}Z+\partial^2 W/\partial X^2+\partial^2 W/\partial Y^2$$
$$+(\Omega/Pr)\cdot(\theta+NC); \quad (6)$$

Energy equation:

$$U\partial\theta/\partial X+V\partial\theta/\partial Y+W\partial\theta/\partial Z$$
$$= (\partial^2\theta/\partial X^2+\partial^2\theta/\partial Y^2)/Pr; \quad (7)$$

Concentration equation:

$$U\partial C/\partial X+V\partial C/\partial Y+W\partial C/\partial Z$$
$$= (\partial^2 W/\partial X^2+\partial^2 W/\partial Y^2)/Sc. \quad (8)$$

A vorticity–velocity method has been successfully developed [27] and will be used for the present study. A vorticity function in the axial direction is defined as:

$$\xi = \partial U/\partial Y-\partial V/\partial X. \quad (9)$$

By differentiating equation (9) and combining with the continuity equation (3), the following equation can be derived:

$$\partial^2 U/\partial X^2+\partial^2 U/\partial Y^2 = \partial\xi/\partial Y-\partial^2 W/\partial X\partial Z, \quad (10)$$

$$\partial^2 V/\partial X^2+\partial^2 V/\partial Y^2 = -\partial\xi/\partial X-\partial^2 W/\partial Y\partial Z. \quad (11)$$

Then the governing equations (3)–(5) can be put into the final vorticity–velocity form. The pressure terms in equations (4) and (5) are eliminated by cross differentiations, and a single equation for the axial vorticity can now be obtained:

$$U\partial\xi/\partial X+V\partial\xi/\partial Y+W\partial\xi/\partial Z+\xi(\partial U/\partial X+\partial V/\partial Y)$$
$$+(\partial W/\partial Y\cdot\partial U/\partial Z-\partial W/\partial X\cdot\partial V/\partial Z)$$
$$= \partial^2\xi/\partial X^2+\partial^2\xi/\partial Y^2-(Ra\cos\delta/Pr)$$
$$\cdot(\partial\theta/\partial X+N\partial C/\partial X). \quad (12)$$

An additional constraint which is used to deduce the axial pressure gradient in axial momentum equation is that global mass conservation at any axial location must be satisfied. This constraint is expressed as:

$$\int_0^{(1+\gamma)/(2\gamma)}\int_0^{(1+\gamma)/4} W\cdot\mathrm{d}X\,\mathrm{d}Y = (1+\gamma)^2/(8\gamma). \quad (13)$$

In summary, the governing equations for the flow include: (i) the axial momentum equation (6); and (ii) the axial vorticity equation (12) and the transverse velocity components (10) and (11). They are of parabolic–elliptic form. This formulation is called the velocity–vorticity method [27]. Flow temperature and concentration are determined by equations (7) and (8), respectively.

Boundary conditions

As mentioned earlier, because of the symmetry about the symmetric plane as shown in Fig. 1, it is sufficient to solve the equations over only the left-hand side of the inclined rectangular duct. The boundary conditions for this domain are given by:

$$U = V = W = 0 \quad \partial\theta/\partial n = \partial C/\partial n = 1$$

at the duct walls, (14a)

$$\partial W/\partial X = U = \partial V/\partial X = \partial\theta/\partial X = \partial C/\partial X = 0$$

at the symmetric plane $X = (1+\gamma)/4$, (14b)

$$W = W_f \quad U = V = \xi = \theta = C = 0$$

at the entrance $Z = 0$. (14c)

The interfacial velocity at the walls as a result of mass diffusion process will be neglected in the analysis. This is because consideration will be given to a situation in which the concentration level is low. The validity and the condition for the neglect of interfacial velocity have been discussed in refs. [28, 29].

After the velocity, temperature and concentration fields are obtained, the computations of the local friction factor, Nusselt number and Sherwood number are of practical interest. Following the usual definitions, the expressions for the product of peripherally average friction factor and Reynolds number fRe, the peripherally averaged Nusselt number Nu and Sherwood number Sh can be written based on the overall force balance for an axial length dZ, the temperature gradient and the concentration gradient at the wall. The expressions are:

$$fRe/(fRe)_0 = (d\bar{P}/dZ)/(d\bar{P}/DZ)_0, \quad (15)$$

$$Nu = 1/[\bar{W}(\overline{\theta_w} - \theta)] \text{ with } \bar{W} = 1, \quad (16)$$

$$Sh = 1/[\bar{W}(\overline{C_w} - C)], \quad (17)$$

where the subscript $_0$ denotes the quantity for purely forced convection. $\overline{\theta_w}$ and $\overline{C_w}$ represent average wall temperature and concentration around the perimeter, respectively.

Governing parameters

The governing equations contain six dimensionless parameters: Ω, Ra^*, N, γ, Pr, and Sc. Ω is a mixed convection parameter defined by equation (2) that contains the ratio of the Rayleigh number Ra to the Reynolds number Re, modified by an inclination angle factor $\sin\delta$. Ra^* is a modified Rayleigh number given by equation (2) and buoyancy ratio N represents the relative effect of chemical species diffusion on the thermal diffusion. When $N = 0$, mass diffusion effect is negligible and the buoyancy force arises solely from the temperature difference. The buoyancy force from mass and thermal diffusion are combined to assist the flow when as $N > 0$, whereas they oppose each other as $N < 0$. An examination of the dimensionless governing equations shows that the inclination angle from the horizontal direction does not explicitly appear in the formulation. Hence, the introduction of the independent parameters Ω and Ra^* has reduced the number of dimensionless parameters from seven to six. Moreover, from equation (2), it is obvious that, as $\delta \to 0$:

$$\sin\delta \to 0, \quad Ra^* \to Ra, \quad \Omega \to 0, \quad (18)$$

and equations (6)–(12) become the governing equations for mixed convection heat and mass transfer in a horizontal rectangular duct [26]. Also, as $\delta \to \pi/2$:

$$\sin\delta \to 1, \quad Ra^* \to 0, \quad \Omega \to Ra/Re, \quad (19)$$

and the buoyancy term in the axial momentum equation (6) becomes $\delta \to \pi/2$:

$$(\Omega/Pr)\cdot(\theta + NC) \to (Gr/Re)\cdot(\theta + NC), \quad (20)$$

which is the correct buoyancy parameter for laminar mixed convection heat and mass transfer in the axial momentum equation in a vertical duct [24, 25].

Thus, it is clear that the introduction of Ω and Ra^* as independent parameters has not only reduced the number of governing parameters of the problem but has permitted a compact formulation in which all inclination angles, including the limiting cases of horizontal and vertical rectangular ducts, can be recovered.

In this work, the results are presented for air ($Pr = 0.7$) over a Schmidt number range of $Sc = 0.2$–2.0. This covers diffusion into air of hydrogen ($Sc = 0.22$), water vapor (0.6), ethanol vapor (1.3) and benzene vapor (2.01) [28, 29]. Ω was varied between 0 and 200 and Ra^* was taken between 0 and 10^5, while buoyancy ratio N was varied between -0.5 and 2.0 with aspect ratios 0.5, 1 and 2.

SOLUTION METHOD

The governing equations are solved numerically by the vorticity–velocity method for three-dimensional parabolic flow [27]. The equations for the unknowns U, V, W, ξ, θ, C and $d\bar{P}/dZ$ are coupled. A numerical finite-difference scheme based on the vorticity–velocity method is used to obtain the solution of equations (6)–(8) and (10)–(12). For given values of Ω, Ra^*, N, Sc, γ, and Pr, the numerical method of solutions for unknown U, V, W, ξ, θ, and C is briefly described below.

(1) The axial velocity at the entrance ($Z = 0$), constrained to $\bar{W} = 1$, is solved independently using an S.O.R. method.

(2) Specify the initial values of U, V, θ and C, and assign a constant for the axial pressure gradient (dP/dZ).

(3) For any axial location, with the known values of U, V and assigned $(d\bar{P}/dZ)$, the axial velocity W at the current position is obtained from equation (6), and the convergence of W can be tested by the satisfaction of the overall conservation of mass, equation (13). If the criterion:

$$\left| \int_0^{(1+\gamma)/(2\gamma)} \int_0^{(1+\gamma)/4} W \cdot dX\, dY - (1+\gamma)^2/(8\gamma) \right| < 10^{-6}, \quad (21)$$

is reached, then the values of $\partial W/\partial X$ and $\partial W/\partial Y$ can be evaluated at each grid point.

(4) The values of $\partial U/\partial Z$ and $\partial V/\partial Z$ are computed using a two-point backward difference formula. With the known values of U, V and W, the new values of ξ, θ and C at the interior points of the next axial position are obtained from equations (12), (7) and (8), respectively, by the Du Fort–Frankel method [30].

(5) The values of $\partial^2 W/\partial X \partial Z$, $\partial^2 W/\partial Y \partial Z$, $\partial \xi/\partial Y$, and $\partial \xi/\partial X$ in equations (10) and (11) are calculated by using the backward difference axially and a central difference in the transverse directions. The elliptic-type equations (10) and (11) are then solved for U and V by an iteration process. During the iteration process, values of vorticity on boundaries are evaluated simultaneously with U and V in the interior region. The boundary vorticity on the wall of $X = 0$ is [16]:

$$\xi_{1,j} = -\xi_{2,j} - 2V_{2,j}/\Delta X + (U_{2,J+1} - U_{2,j-1})/(2\Delta Y). \quad (22)$$

It is noted that the boundary vorticities on the other walls can also be computed in a similar expression.

(6) Steps (3)–(5) are repeated at a cross-section until the following criterion is satisfied for the velocity components U and V,

$$\varepsilon = \mathrm{Max}|\phi_{i,j}^{m+1} - \phi_{i,j}^{m}|/\mathrm{Max}|\phi_{i,j}^{m+1}| < 10^{-5}, \quad \phi = U \text{ or } V \quad (23)$$

where m is the mth iteration of steps (3)–(5).

(7) The peripherally averaged friction factor, Nusselt number and Sherwood number are determined from equations (15)–(17).

(8) Steps (3)–(7) are repeated at next axial location until the final axial location of interest is reached.

To ensure the accuracy of the present numerical results, a numerical experiment with uniform grids was made on the mesh size $I \times J$ and axial step size ΔZ^* to determine the grid size required for acceptable accuracy. Four arrangements of grid points in the x, y and z directions are tested and corresponding results are presented in Table 1. It is found that the deviation in Nu calculated with $I \times J = 16 \times 32$ and 24×48 ($\Delta Z^* = 1 \times 10^{-4}$–$2.5 \times 10^{-4}$) is always less than 1%. Furthermore, the deviation in Nu calculated using $I \times J$ (ΔZ^*) = 16×32 (2×10^{-5}–2.5×10^{-4}) and 16×32 (1×10^{-4}–2.5×10^{-4}) are estimated to be within 1%. Thus, the computations involving an $I \times J$ (ΔZ^*) = 16×32 (1×10^{-4}–2.5×10^{-4}) grid are considered to be sufficiently accurate to describe the heat and mass transfer in inclined rectangular ducts. All the results presented in the next section are computed using the latter grid.

RESULTS AND DISCUSSION

(a) *Effects of mixed convection parameter* Ω

The buoyancy effects on the flow characteristics in inclined channels are usually presented by the friction factor ratio $fRe/(fRe)_0$, where the subscript $_0$ represents the quantity for purely forced convection. Figure 2 shows the axial variations of $fRe/(fRe)_0$ for different values of Ω at $Ra^* = 5 \times 10^4$, $N = 1$, $Sc = 1.3$ and $\gamma = 1$. For clear illustration, the results near the entrance are specifically plotted in the inset in Fig. 2. The purely forced convection curve, denoted by E in Fig. 2, has been obtained by setting Ω and Ra^* to be zero. In Fig. 2, near the inlet, the buoyancy effects are insignificant and all the curves follow the forced convection curve [i.e. the line of $fRe/(fRe)_0 = 1$]. As the buoyancy effects become important, each curve of the friction factor ratio branches out from the line of $fRe/(fRe)_0 = 1$. The buoyancy effects are the most pronounced at the highest value of Ω since this parameter represents a ratio of natural convection to forced convection effects. At $\Omega = 200$, the maximum value of $fRe/(fRe)_0$ occurs at approximately $Z^* = 2.5 \times 10^{-2}$. The occurrence of the maximum

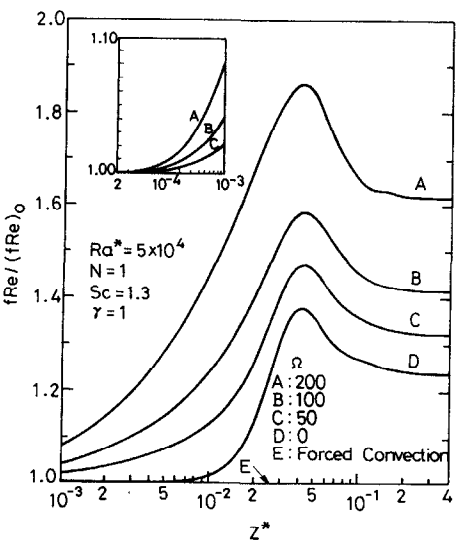

FIG. 2. The axial variations of the local friction factor ratio for $Ra^* = 5 \times 10^4$, $N = 1$, $Sc = 1.3$ and $\gamma = 1$ with Ω as parameter.

Table 1. Comparisons of local Nusselt number Nu for various grid arrangements for the case of $Pr = 0.7$, $Ra^* = 5 \times 10^4$, $\Omega = 100$, $N = 1$, $Sc = 1.3$ and $\gamma = 1$

$I \times J$ (ΔZ^*)	Z^* 0.006	0.01	0.02	0.04	0.06	0.1	0.4
12×24 (1.0×10^{-4}–2.5×10^{-4})	5.698	5.034	4.622	5.231	5.394	5.438	5.468
16×32 (1.0×10^{-4}–2.5×10^{-4})	5.761	5.072	4.633	5.246	5.431	5.457	5.486
16×32 (2.0×10^{-5}–2.5×10^{-4})	5.722	5.071	4.622	5.237	5.434	5.458	5.486
24×48 (1.0×10^{-4}–2.5×10^{-4})	5.804	5.095	4.636	5.259	5.464	5.471	5.498

local friction factor is closely related to the appearance of a local maximum secondary flow intensity [18]. After reaching a maximum value, the curve decreases and approaches a limiting value when the velocity profile becomes fully developed. It may be noted that, for $\Omega = 200$, the enhancement in flow resistance can be as much as 80%.

The axial variations of Nu and Sh with Ω as parameter are shown in Fig. 3. For comparison, the results near the inlet are plotted in the inset. Due to the entrance effect, a monotonic decrease in local Nusselt (Sherwood) number near the entrance is noted. The onset of buoyancy effects occurs at a specific distance from the entrance which depends upon Ω. For each curve shown in Fig. 3, a minimum local Nu (Sh) exists. The location of the minimum Nu (Sh) is a result of combined entrance and buoyancy effects [7]. After reaching the first minimum in Nu, maximum and minimum local Nu may exist for some cases. Finally, the curves of Nu approach asymptotic values when the temperature profiles become fully developed. The first minimum in Nu and the subsequent maximum and minimum are also found in the results of mixed convection heat transfer in a horizontal duct [14] and a horizontal tube [17]. In addition, it is found that the value of Sh is larger than that of Nu. This is due to the fact that the Schmidt number ($Sc = 1.3$) is larger than the Prandtl number ($Pr = 0.7$) in the flow system.

(b) *Effects of modified Rayleigh number* Ra*

Figure 4 shows the axial variations of Nu and Sh for different modified Rayleigh number Ra^* at $\Omega = 100$, $N = 1$, $Sc = 1.3$ and $\gamma = 1$. From the defining equations of Ra^* and Ω [equation (2)] it is seen that holding Ω fixed while increasing Ra^* is like decreasing the inclination angle δ and simultaneously increasing the Rayleigh number Ra. Alternatively, the same effect can be obtained at a fixed inclination angle δ by increasing Ra and Re simultaneously such that the value of Ω remains the same. In any case, the effect of increasing Ra^* at a fixed Ω is to increase the combined buoyancy effects. It is seen that the effect of Ra^* is practically negligible when $Ra^* \leqslant 10^3$. The decrease

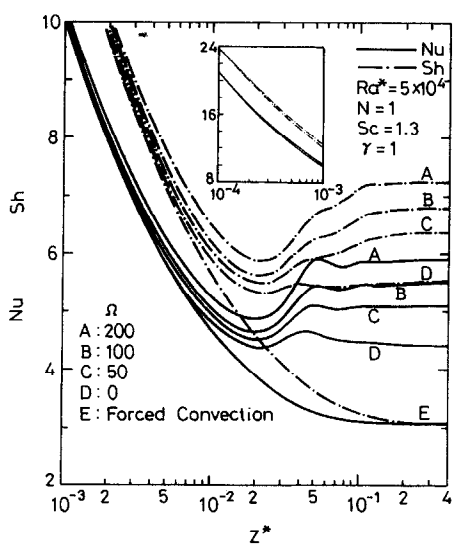

FIG. 3. The axial variations of the local Nusselt and Sherwood numbers for $Ra^* = 5 \times 10^4$, $N = 1$, $Sc = 1.3$ and $\gamma = 1$ with Ω as parameter.

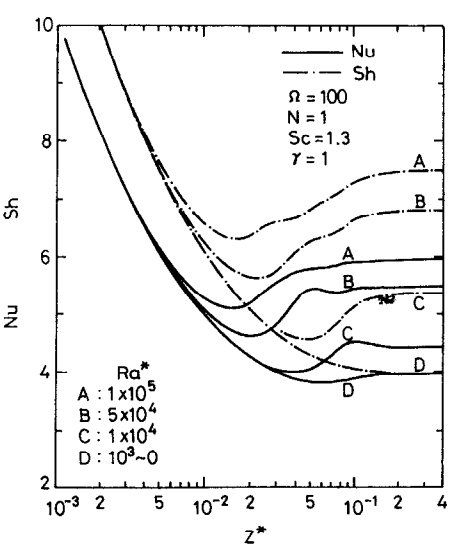

FIG. 4. The axial variations of the local Nusselt and Sherwood numbers for $\Omega = 100$, $N = 1$, $Sc = 1.3$ and $\gamma = 1$ with Ra^* as parameter.

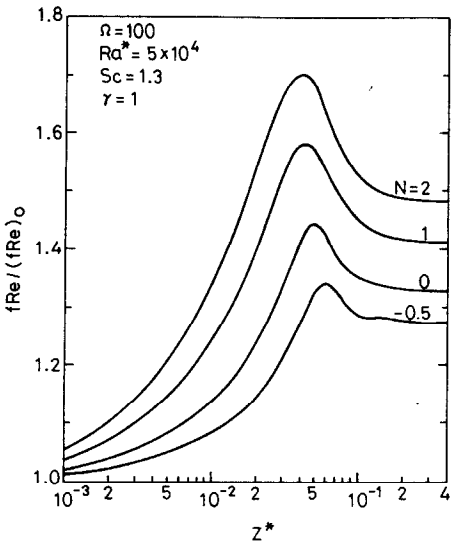

FIG. 5. The axial variations of the local friction factor ratio for $\Omega = 100$, $Ra^* = 5 \times 10^4$, $Sc = 1.3$ and $\gamma = 1$ with N as parameter.

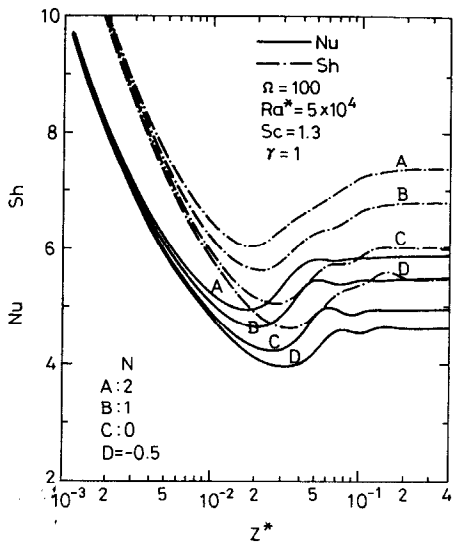

FIG. 6. The axial variations of the local Nusselt and Sherwood numbers for $\Omega = 100$, $Ra^* = 5 \times 10^4$, $Sc = 1.3$ and $\gamma = 1$ with N as parameter.

of Nu (Sh) in the entrance region is known to be the entrance effect and the deviation from the results of $Ra^* = 0$ is due to the buoyancy effects. It is clear that the entrance and buoyancy effects will eventually balance out and the local minimum Nu (Sh) appears at some downstream location depending on the value of Ra^*. Subsequently, the buoyancy effect dominates over the entrance effect and Nu (Sh) increases. Finally, Nu (Sh) approaches an asymptotic value when the temperature (concentration) profile becomes fully developed.

(c) *Effects of buoyancy ratio* N

The effects of buoyancy ratio N on the variations of local $fRe/(fRe)_0$, Nu and Sh are presented in Figs. 5 and 6. It is seen that, as compared to the case of $N = 0$ (i.e. the case in which there is no solutal buoyancy effect and the buoyancy force arises solely from the thermal variations), the local friction factor, local Nusselt and Sherwood numbers increase when the buoyancy force from species diffusion acts in the same direction as the thermal buoyancy force to assist the flow (i.e. $N > 0$) and decrease when the solutal buoyancy force acts in the opposite direction of the thermal buoyancy force to oppose the flow (i.e. $N < 0$). Indeed, the combined effects of thermal and solutal diffusion are represented by the term $\theta + NC$ in equation (6). When the combination of Ω, Ra^*, N, Sc, γ and Pr is such that $\theta + NC > \theta$, the net buoyancy force contributes to an increase in the friction factor ratio, local Nusselt and Sherwood numbers beyond their respective values for $N = 0$. On the other hand, if $\theta + NC < \theta$, the net buoyancy force will contribute to a decrease in these three quantities below those for $N = 0$. Inspection of Figs. 5 and 6 further indicates that the location at which enhancement begins advances upstream with increasing N. This effect is due to the increase in the combined buoyancy effects of thermal and solutal diffusion.

(d) *Effects of Schmidt number* Sc

Figure 7 gives the effects of Schmidt number on the Nusselt and Sherwood numbers. It is apparent that

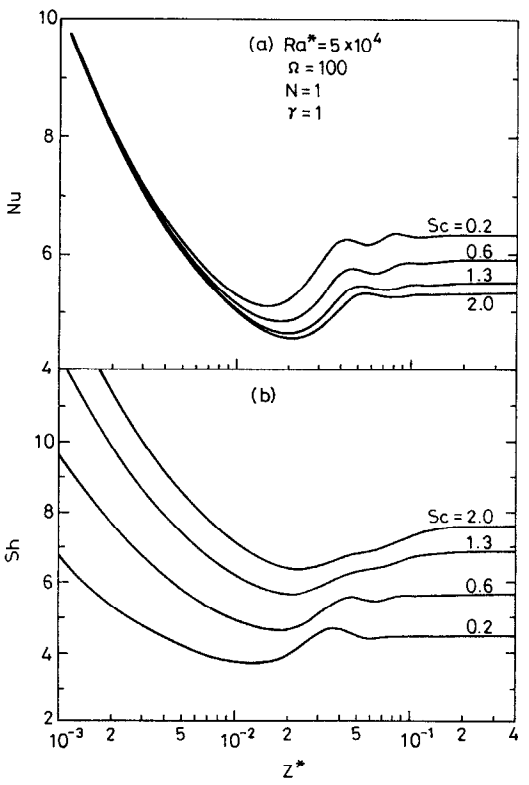

FIG. 7. The axial variations of the local Nusselt and Sherwood numbers for $\Omega = 100$, $Ra^* = 5 \times 10^4$, $N = 1$ and $\gamma = 1$ with Sc as parameter.

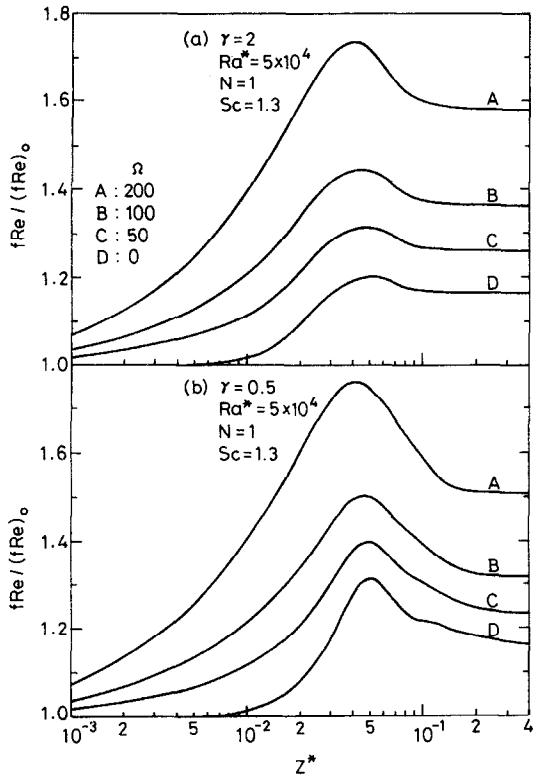

FIG. 8. The axial variations of the local friction factor ratio with Ω as parameter for: (a) $\gamma = 2$; and (b) $\gamma = 0.5$.

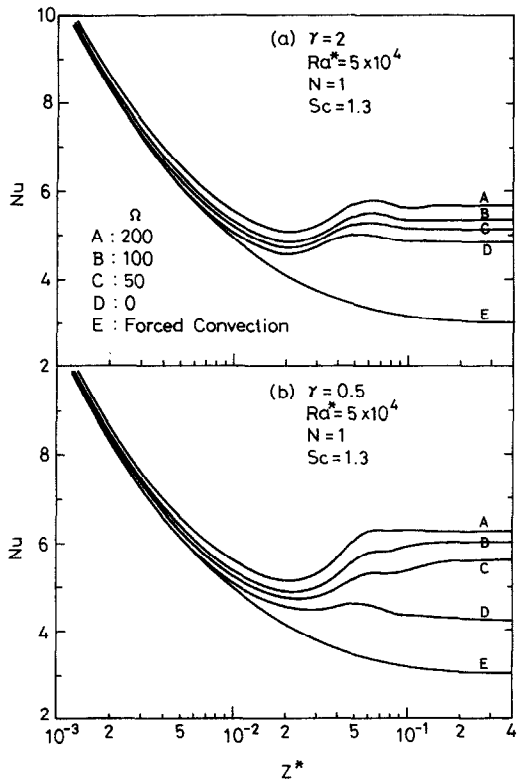

FIG. 9. The axial variations of the local Nusselt number with Ω as parameter for: (a) $\gamma = 2$; and (b) $\gamma = 0.5$.

the axial distance of the occurrence of the onset of buoyancy effects is shorter with a smaller value of *Sc*. Additionally, a larger *Nu* is noted for a system with a smaller *Sc*. This is because a smaller *Sc* corresponds to a larger binary diffusion coefficient, which in turn exerts a larger influence on the flow field and hence the thermal field. The Sherwood number results, Fig. 7b, indicate that, for a given Ω, Ra^*, *N* and γ, a larger *Sh* is associated with a larger *Sc*. That is, the mass transfer rate increases with increasing Schmidt number. The reason for this is that a larger Schmidt number corresponds to a smaller binary diffusion coefficient in a given mixture and hence a thinner concentration boundary-layer thickness relative to the flow boundary-layer thickness. This results in a larger mass transfer rate at the duct walls or a larger Sherwood number.

(e) *Effects of aspect ratio* γ

The effect of the aspect ratio of a rectangular duct on frictional factor and heat transfer results is of practical interest. The local *fRe* and *Nu* for the aspect ratios $\gamma = 2$ and 0.5 are shown in Figs. 8 and 9, respectively, with mixed convection parameter Ω as parameter. In Fig. 9a and b, the lowest curve can be regarded as a limiting case for purely forced convection. Comparing Figs. 2 and 8 or Figs. 3 and 9, it is found that the general behaviors of the $fRe/(fRe)_0$ and *Nu* for aspect ratios $\gamma = 2$ and 0.5 are qualitatively similar to those of $\gamma = 1$. However, the maximum values of the $fRe/(fRe)_0$ and *Nu* of square channel (i.e. $\gamma = 1$) are higher than those with $\gamma = 2$ and 0.5. This is due to the greater secondary effects for $\gamma = 1$ in an inclined rectangular duct.

(f) *Comparisons with numerical and experimental results*

Since no experimental or numerical data for mixed convection heat and mass transfer in inclined rectangular ducts are available in the literature, comparisons have been made for the limiting case of mixed convection heat transfer in a horizontal duct without mass buoyancy effect. Table 2 presents a comparison of the calculated Nusselt numbers with the numerical results of Chou and Hwang [16]. It is found that the differences in the local Nusselt number *Nu* are all less than 1% at every axial location. Additionally, the comparisons of the limiting case of developing mixed convection heat transfer in an inclined rectangular duct were also made. The good agreement between the experimental and numerical results in the fully developed region is clearly depicted in Fig. 10. However, the deviations between the predicted results and the available experimental results are relatively significant in the entrance region. This is due to the fact that, in the present work, the effect of wall conduction is neglected. In fact, the circumferential wall conduction would increase the already established secondary flow which, in turn, enhances the value of *Nu* [21].

Table 2. Comparisons of the local Nusselt numbers between the present predictions and those of Chou and Hwang for $Pr = 0.7$, $Ra^* = 6 \times 10^4$, $\Omega = 0$ and $N = 0$

	Z^*				
	0.01	0.03	0.05	0.07	0.1
Present work	4.758	4.185	4.555	4.460	4.415
Chou and Hwang [16]	4.759	4.191	4.561	4.465	4.408

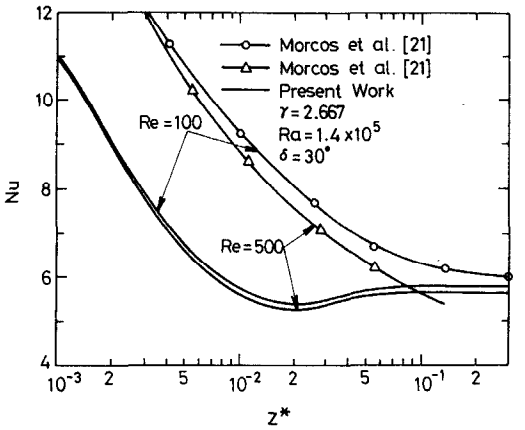

FIG. 10. Comparisons between the predicted Nu and the available experimental results [21] for mixed convection heat transfer in an inclined rectangular duct with $\delta = 30°$.

CONCLUSION

Laminar mixed convection heat and mass transfer in inclined rectangular ducts has been studied. The effects of the modified Rayleigh number Ra^*, buoyancy ratio N, Schmidt number Sc, aspect ratio γ and Ω, a parameter that measures the relative importance of free and forced convection, on the momentum, heat and mass transfer were examined in detail. What follows is brief summary of the major results.

(1) Variations of local friction factor ratios, local Nusselt and Sherwood numbers show that the axial position corresponding to the onset of the buoyancy effects depends mainly on the magnitude of Ω and Ra^*.

(2) The distributions of local Nusselt (Sherwood) number are characterized by a decay near the entrance due to the entrance effect; but the decay is attenuated by the onset of buoyancy-driven secondary flows. After a first local minimum being reached, maximum and minimum local Nusselt number may exist. Finally, Nu approaches an asymptotic value when the temperature profile becomes fully developed.

(3) The local friction factor, local Nusselt and Sherwood numbers are found to increase and decrease when the buoyancy force from species diffusion assists and opposes, respectively, the thermal buoyancy force.

(4) A larger Nu is experienced for a system with a smaller Sc.

Acknowledgement—The financial support of this research by the National Science Council, R.O.C., under the contract NSC 82-0401-E211-003 is greatly appreciated.

REFERENCES

1. K. C. Cheng and G. J. Hwang, Numerical solution for combined free and forced laminar convection in horizontal rectangular channels, *J. Heat Transfer* **91**, 59–66 (1969).
2. F. C. Chou and G. J. Hwang, Combined free and forced laminar convection in horizontal rectangular channels for high ReRa, *Can. J. Chem. Eng.* **62**, 830–836 (1984).
3. M. Iqbal and J. W. Stachiewicz, Influence of tube orientation on combined free and forced laminar convection heat transfer, *J. Heat Transfer* **88**, 109–116 (1966).
4. K. C. Cheng and S. W. Hong, Combined free and forced laminar convection in inclined tubes, *Appl. Scient. Res.* **27**, 19–38 (1972).
5. K. Futagami and F. Abe, Combined forced and free convection heat transfer in an inclined tube (1st report, laminar region), *Trans. Japan. Soc. Mech. Engrs* **38**, 1799–1811 (1972).
6. J. W. Ou, K. C. Cheng and R. C. Lin, Combined free and forced laminar convection in inclined rectangular channels, *Int. J. Heat Mass Transfer* **19**, 277–283 (1976).
7. K. C. Cheng, S. W. Hong and G. J. Hwang, Buoyancy effects on laminar heat transfer in the thermal entrance region of horizontal rectangular channels with uniform wall heat flux for large Prandtl number fluid, *Int. J. Heat Mass Transfer* **15**, 1819–1836 (1972).
8. J. W. Ou, K. C. Cheng and R. C. Lin, Natural convection effects on Graetz problem in horizontal rectangular channels with uniform wall temperature for large Pr. *Int. J. Heat Mass Transfer* **17**, 835–843 (1974).
9. C. A. Hieber and S. K. Sreenivasan, Mixed convection in an isothermally heated horizontal pipe, *Int. J. Heat Mass Transfer* **17**, 1337–1348 (1974).
10. J. W. Ou and K. C. Cheng, Natural convection effects on Graetz problem in horizontal isothermal tubes, *Int. J. Heat Mass Transfer* **20**, 953–960 (1977).
11. M. Hishida, Y. Nagano and M. S. Montesclaros, Combined forced and free convection in the entrance region of an isothermally heated horizontal pipe, *J. Heat Transfer* **104**, 153–159 (1982).
12. M. M. M. Abou-Ellail and S. M. Morcos, Buoyancy effects in the entrance region of horizontal rectangular channels, *J. Heat Transfer* **105**, 924–928 (1983).
13. F. P. Incropera and J. A. Schutt, Numerical simulation of laminar mixed convection in the entrance region of horizontal rectangular ducts, *Numer. Heat Transfer* **8**, 707–729 (1985).
14. F. P. Incropera, A. L. Knox and J. R. Maughan, Mixed convection flow and heat transfer in the entry region of a horizontal rectangular duct, *J. Heat Transfer* **109**, 434–439 (1987).
15. H. V. Mahaney, F. P. Incropera and S. Ramadhyani, Development of laminar mixed convection flow in a horizontal rectangular duct with uniform bottom heating, *Numer. Heat Transfer* **12**, 137–155 (1987).
16. F. C. Chou and G. J. Hwang, Vorticity–velocity method

for Graetz problem with the effect of natural convection in a horizontal rectangular channel with uniform wall heat flux, *J. Heat Transfer* **109,** 704–710 (1987).
17. F. C. Chou and G. J. Hwang, Numerical analysis of the Graetz problem with natural convection in a uniformly heated horizontal tube, *Int. J. Heat Mass Transfer* **31,** 1299–1308 (1988).
18. J. N. Lin and F. C. Chou, Laminar mixed convection in the thermal entrance region of horizontal isothermal rectangular channels, *Can. J. Chem. Eng.* **67,** 361–367 (1989).
19. M. M. M. Abou-Ellail and S. M. Morcos, Combined forced and free laminar convection in the entrance region of inclined rectangular channels. In *Proceedings of the International Conference on Numerical Methods for Non-Linear Problems* (Edited by C. Taylor *et al.*), pp. 807–821. Pineridge Press, Swansea (1980).
20. K. C. Cheng and F. P. Yuen, Flow visualization studies on secondary flow pattern for mixed convection in the entrance region of isothermally heated inclined pipes, *Fundamentals of Forced and Mixed Convection, ASME HTD* **42,** 121–130 (1985).
21. S. M. Morcos, M. M. Hilal, M. M. Kamel and M. S. Soliman, Experimental investigation of mixed laminar convection in the entrance region of inclined rectangular channels, *J. Heat Transfer* **108,** 574–579 (1986).
22. D. Choudhury and S. V. Patankar, Combined forced and free laminar convection in the entrance region of an inclined isothermal tube, *J. Heat Transfer* **110,** 901–909 (1988).
23. F. Santarelli and F. P. Foraboschi, Heat transfer in laminar mixed convection in a reacting fluid, *Chem. Eng.* **6,** 59–68 (1973).
24. W. M. Yan, Mixed convection heat transfer enhancement through latent heat transport in vertical parallel plate channel flows, *Can. J. Chem. Eng.* **69,** 1277–1282 (1991).
25. W. M. Yan, Effects of film evaporation on laminar mixed convection heat and mass transfer in a vertical channel, *Int. J. Heat Mass Transfer* **35,** 3419–3429 (1992).
26. J. N. Lin, F. C. Chou, W. M. Yan and P. Y. Tzeng, Combined buoyancy effects of thermal and mass diffusion on laminar forced convection in the thermal entrance region of horizontal square channels, *Can. J. Chem. Eng.* **79,** 681–689 (1992).
27. K. Ramakrishna, S. G. Rubin and P. K. Khosla, Laminar natural convection along vertical square ducts, *Numer. Heat Transfer* **5,** 59–79 (1982).
28. B. Gebhart and L. Pera, The nature of vertical convection flows resulting from the combined buoyancy effects of thermal and mass diffusion, *Int. J. Heat Mass Transfer* **14,** 2025–2050 (1971).
29. T. S. Chen and C. F. Yuh, Combined heat and mass transfer in natural convection along a vertical cylinder, *Int. J. Heat Mass Transfer* **23,** 451 461 (1980).
30. P. J. Roache, *Computational Fluid Dynamics*, pp. 61–64. Reinhold, New York (1971).